Electronic Supplementary Material (ESI) for Green Chemistry.

Supporting Information

Facet-dependent electrocatalytic oxidation activity of Co_3O_4 nanocrystals for 5-hydroxymethylfurfural

Zhenchuan Zhang,[a] Zhaohui Yang,[a] Chenyang Wei,[a] Zhenghui Liu,[b] and Tiancheng Mu*[a]

[a] Department of Chemistry, Renmin University of China, Beijing 100872, China, Email: tcmu@ruc.edu.cn

[b] Department of Chemistry, Taizhou University, Taizhou 318000, Zhejiang, China.

1. Supplementary Figures

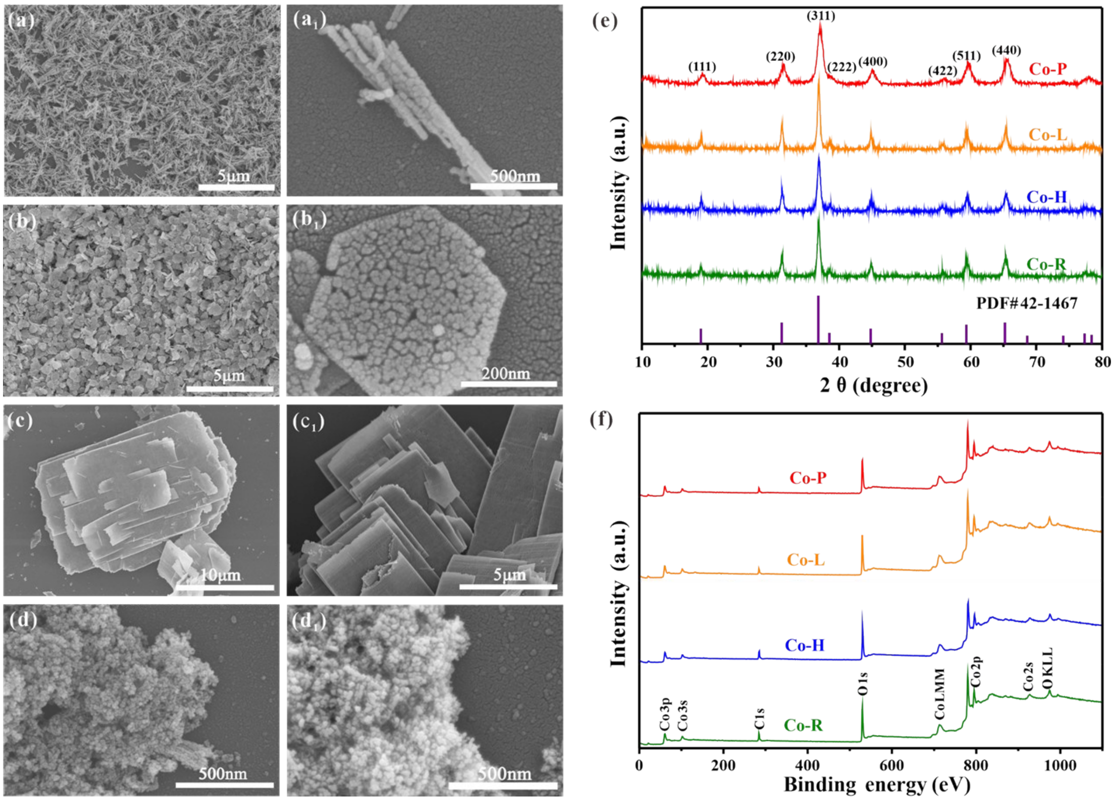

Fig. S1. SEM image of Co-R (a and a_1), Co-H (b and b_1), Co-L (c and c_1) and Co-P (d and d_1). XRD pattern (e) and XPS survey spectra (f) of synthesized catalysts.

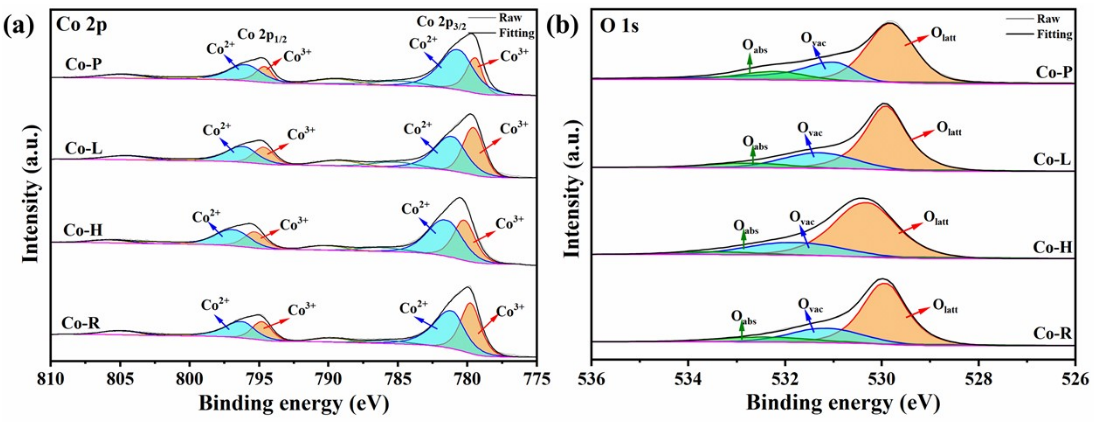

Fig. S2. (a) Co 2p and (b) O 1s XPS spectra of synthesized catalysts.

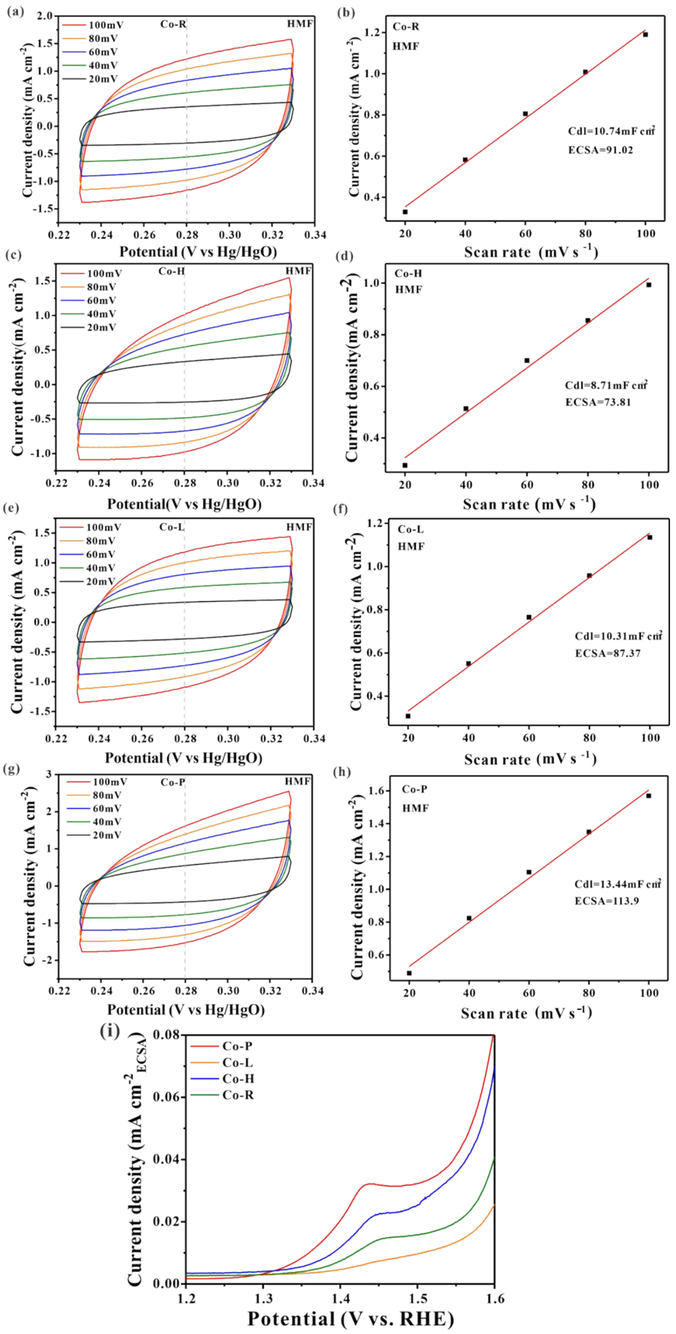

Fig. S3. Cyclic voltammograms (CVs) obtained with Co-R (a), Co-H (c), Co-L (e) and Co-P (g) in 1.0 M KOH with 10 mM HMF at scan rates of 20, 40, 60, 80 and 100 mV, respectively. Change of current density plotted against scan rate for Co-R (b), Co-H (d), Co-L (f) and Co-P (h) in 1.0 M KOH with 10 mM HMF. (i) The LSV curves of Co_3O_4 NCs by ECSA normalization at a scan rate of 5 mV s^{-1} in 1.0 M KOH with 10 mM HMF. The linear slope (b, d, f, and h) is equivalent to the double-layer capacitance Cdl. The corresponding ECSA value is calculated via the equation ECSA = Cdl/Cs, where the specific capacitance value (Cs) was 118 μF cm^{-2}.

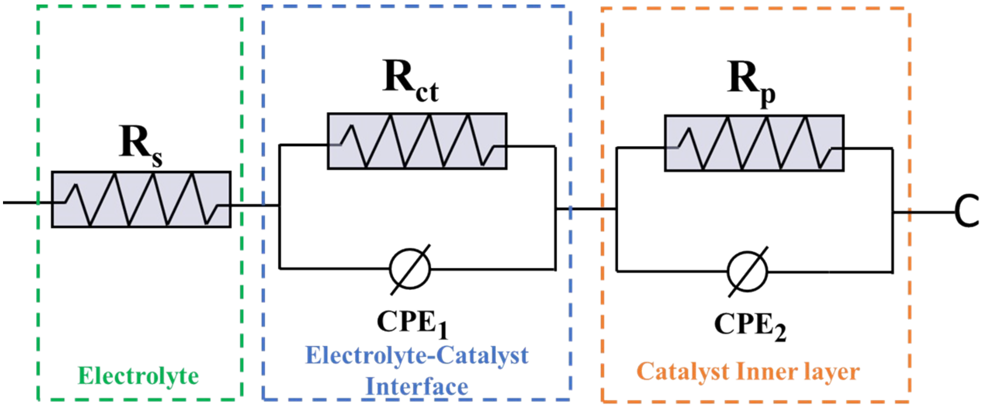

Fig. S4. The equivalent circuit image. R_s stands for solution resistance. CPE_1 represents double-layer capacitance. R_{ct} has contact with the interfacial charge transfer reaction. CPE_2 and R_p are related to the dielectric properties and the resistance of the electrode film.

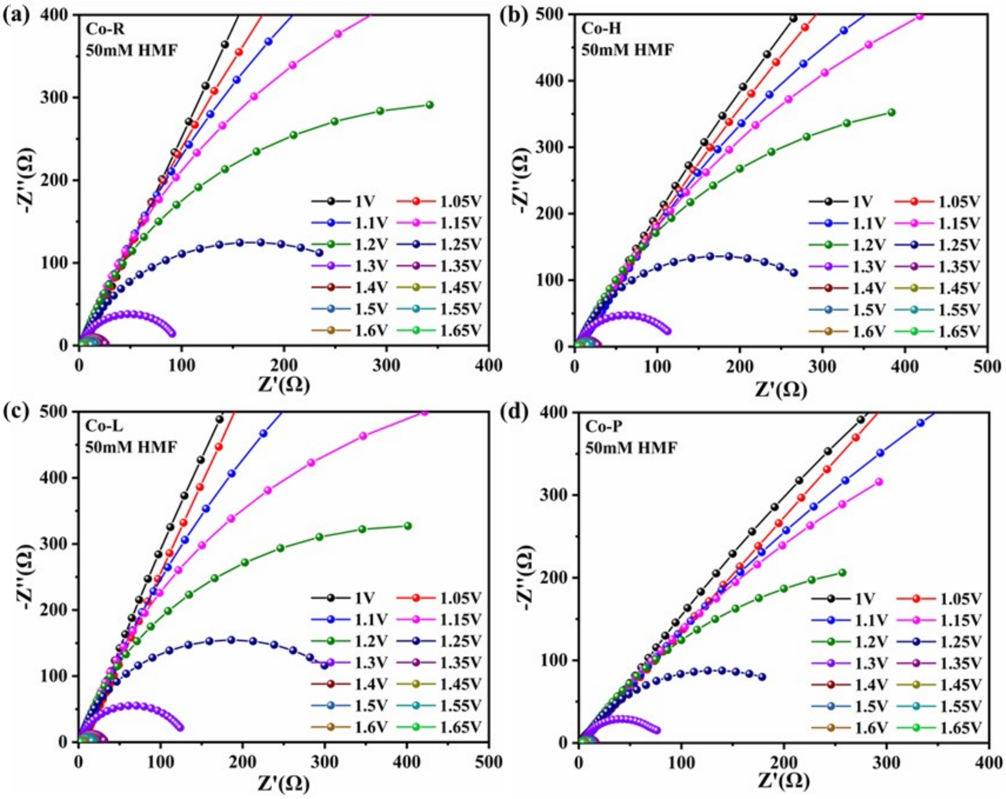

Fig. S5. In operando EIS. The corresponding Nyquist plots of Co-R (a), Co-H (b), Co-L (c) and Co-P (d) at various voltages in 1.0 M KOH with 50 mM HMF.

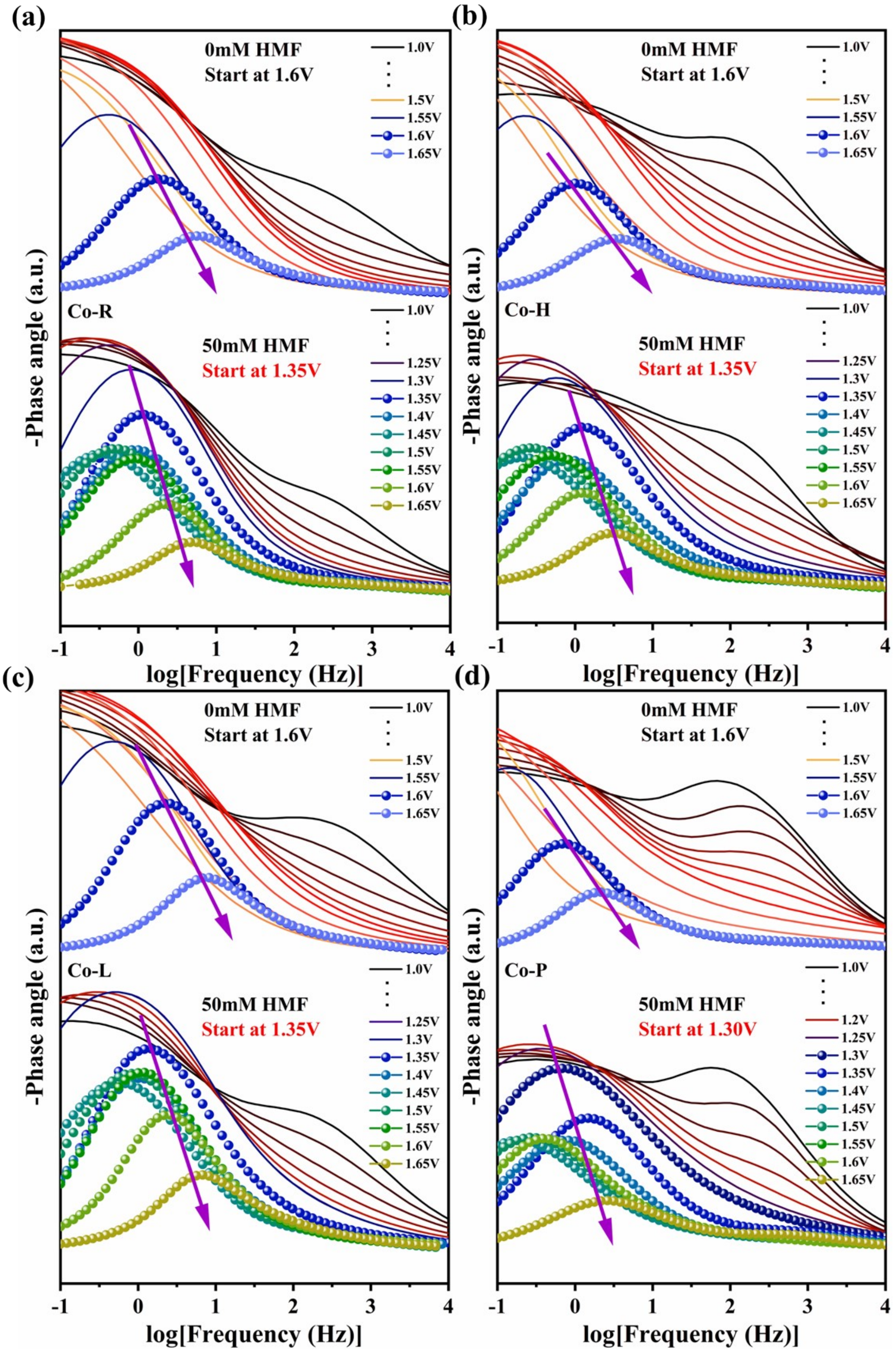

Fig. S6. In operando EIS. The corresponding Bode phase plots of Co-R (a), Co-H (b), Co-L (c) and Co-P (d) at various voltages in 1.0 M KOH with 50 mM HMF.

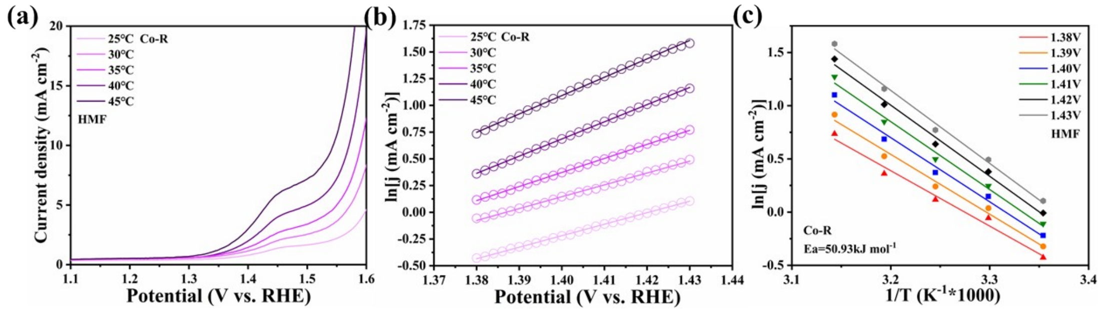

Fig. S7. (a) LSV curves obtained at different temperatures T on Co-R in 1.0 M KOH with 10 mM at a potential sweep rate of 5 mV s^{-1}. (b) The semilogarithmic plots of j vs. RHE obtained at different T on Co-R. (c) Arrhenius plots ln j (A) versus 1/T (K^{-1}) for the HMFOR on the Co-R electrode at different potentials. The Ea values were calculated according to Arrhenius equation: $Inj = InA - ({}^{Ea}/{}_{R})\frac{1}{T}$, Where A is pre-exponential factor, Ea is activation energy, R is gas constant and T is the temperature (kelvin).

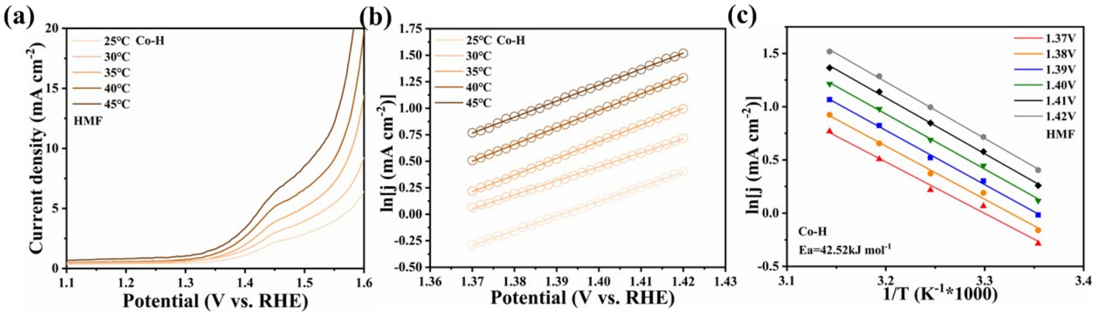

Fig. S8. (a) LSV curves obtained at different T on Co-H in 1.0 M KOH with 10 mM at a potential sweep rate of 5 mV s^{-1}. (b) The semilogarithmic plots of j vs. RHE obtained at different T on Co-H. (c) Arrhenius plots ln j (A) versus 1/T (K^{-1}) for the HMFOR on the Co-H electrode at different potentials.

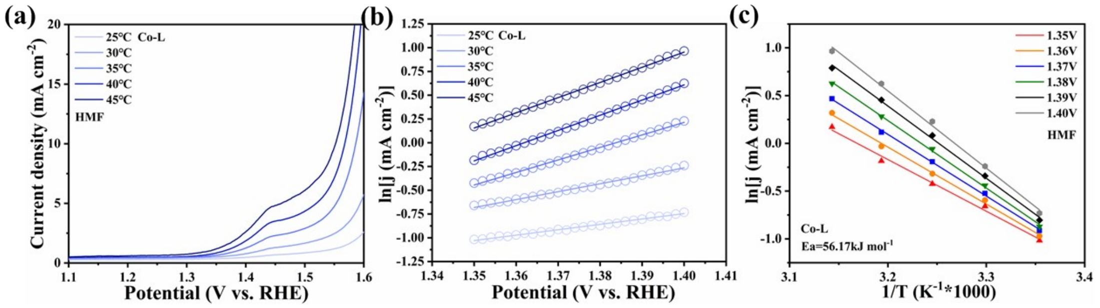

Fig. S9. (a) LSV curves obtained at different T on Co-L in 1.0 M KOH with 10 mM at a potential sweep rate of 5 mV s^{-1}. (b) The semilogarithmic plots of j vs. RHE obtained at different T on Co-L. (c) Arrhenius plots ln j (A) versus 1/T (K^{-1}) for the HMFOR on the Co-L electrode at different potentials.

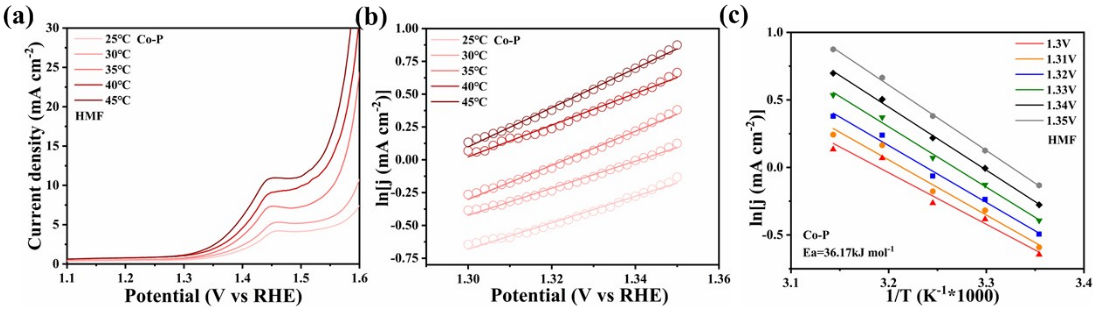

Fig. S10. (a) LSV curves obtained at different T on Co-P in 1.0 M KOH with 10 mM at a potential sweep rate of 5 mV s^{-1}. (b) The semilogarithmic plots of j vs. RHE obtained at different T on Co-P. (c) Arrhenius plots ln j (A) versus 1/T (K^{-1}) for the HMFOR on the Co-P electrode at different potentials.

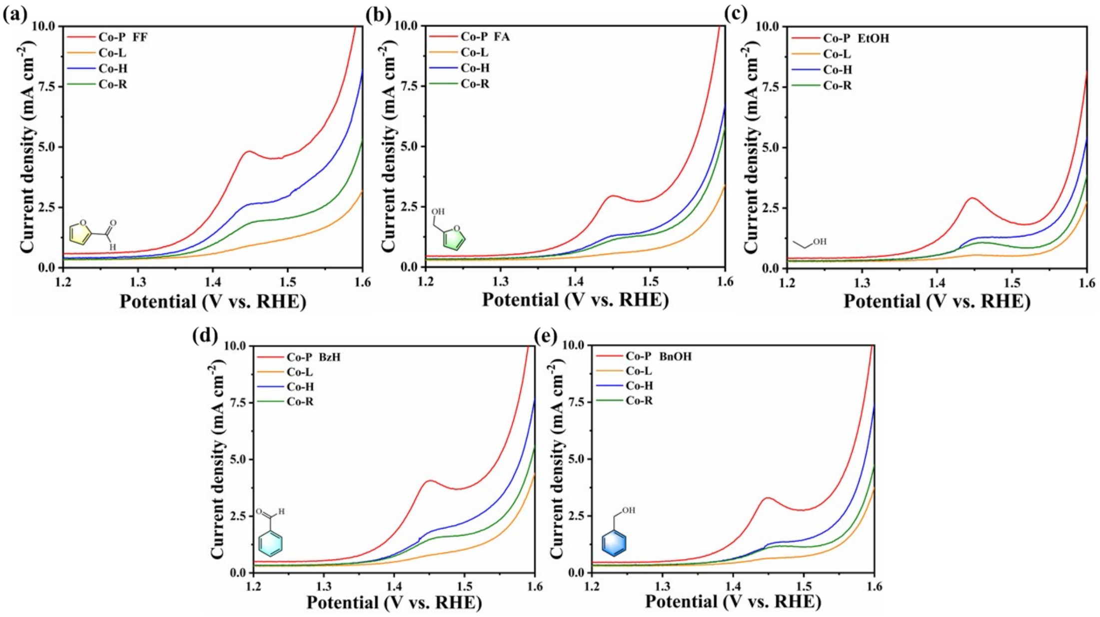

Fig. S11. The LSV curves of Co_3O_4 NCs at a scan rate of 5 mV s^{-1} in 1.0 M KOH with 10 mM (FF), (FA), (EtOH), (BzH) and (BnOH).

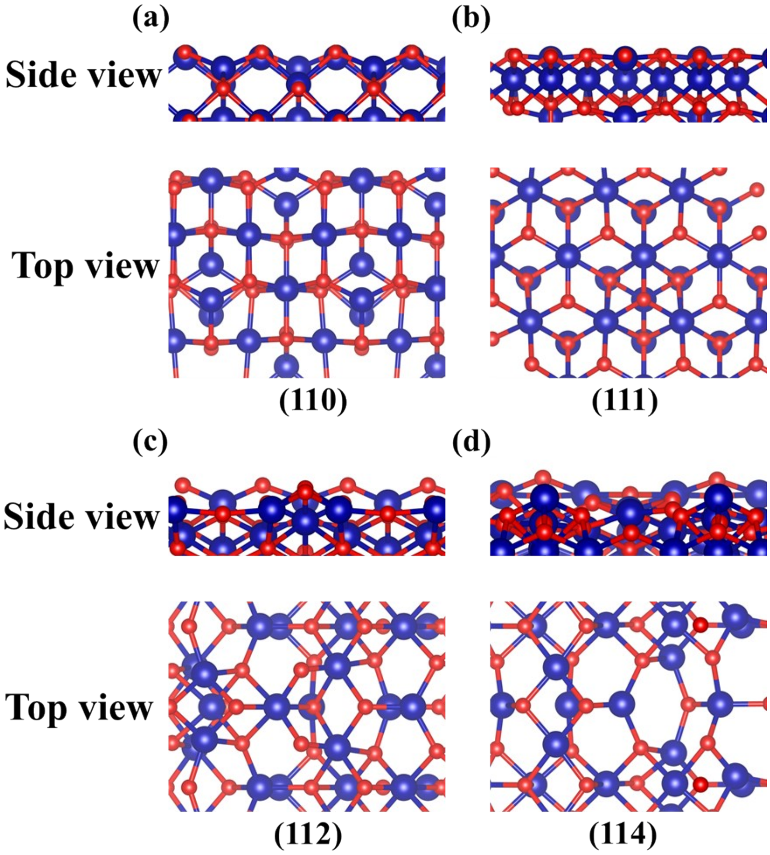

Fig. S12. The structures of (110) (a), (111) (b), (112) (c), and (114) (d) facets of Co_3O_4. The blue and red spheres represent Co and O, respectively.

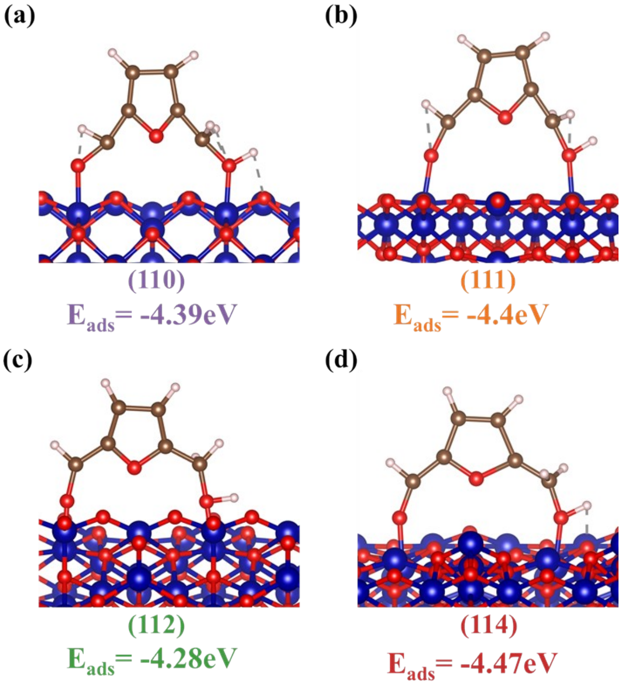

Fig. S13. Figures (a) to (d) show the optimal adsorption configuration and energy (E_{ads}) of HMF on Co-R, Co-H, Co-L and Co-P obtained by DFT calculations. The blue, red and white spheres represent Co, O and H, respectively.

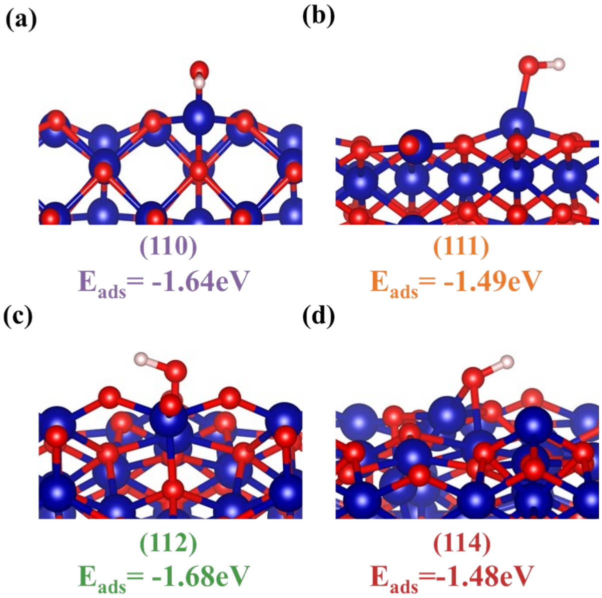

Fig. S14. Figures (a) to (d) show the optimal adsorption configuration and energy (E_{ads}) of OH^- on Co-R, Co-H, Co-L and Co-P obtained by DFT calculations. The blue, red and white spheres represent Co, O and H, respectively.

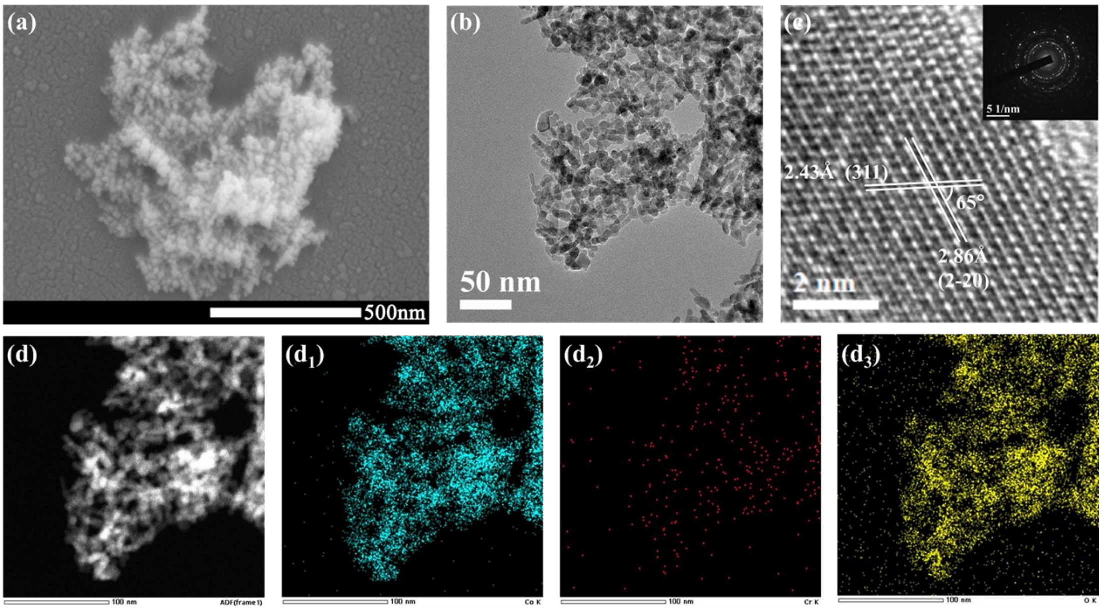

Fig. S15. SEM and TEM image of 0.6wt% Cr-doped Co-P (a and b). (c and inset c) the corresponding high-resolution images and SAED patterns. (d-d_3) Corresponding elemental mappings of 0.6wt% Cr-doped Co-P with Co (d_1), Cr (d_2) and O (d_3).

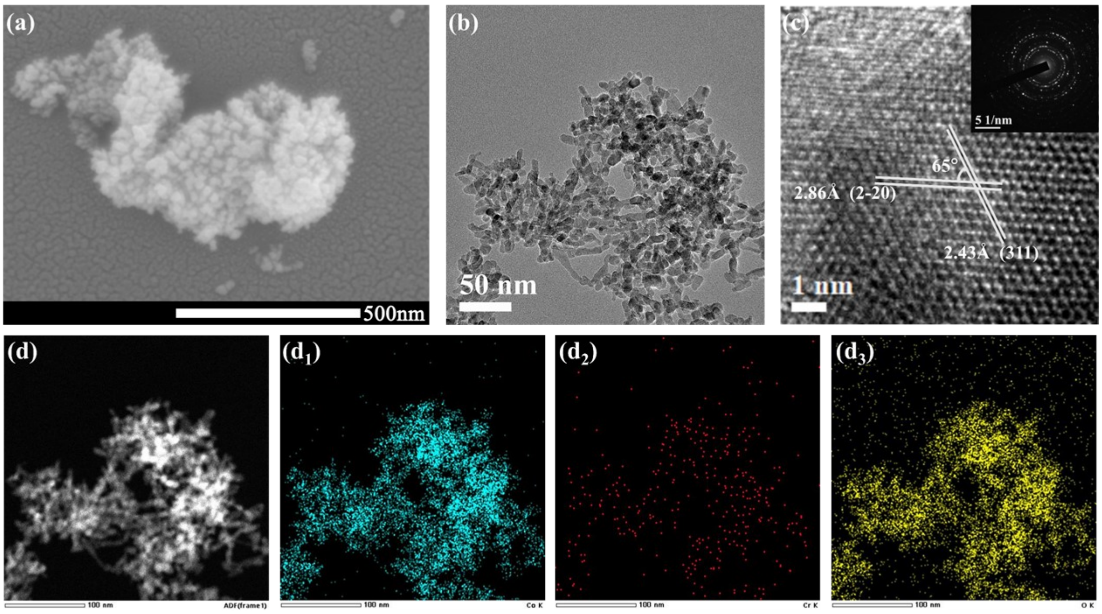

Fig. S16. SEM and TEM image of 2.1wt% Cr-doped Co-P (a and b). (c and inset c) the corresponding high-resolution images and SAED patterns. (d-d_3) Corresponding elemental mappings of 2.1wt% Cr-doped Co-P with Co (d_1), Cr (d_2) and O (d_3).

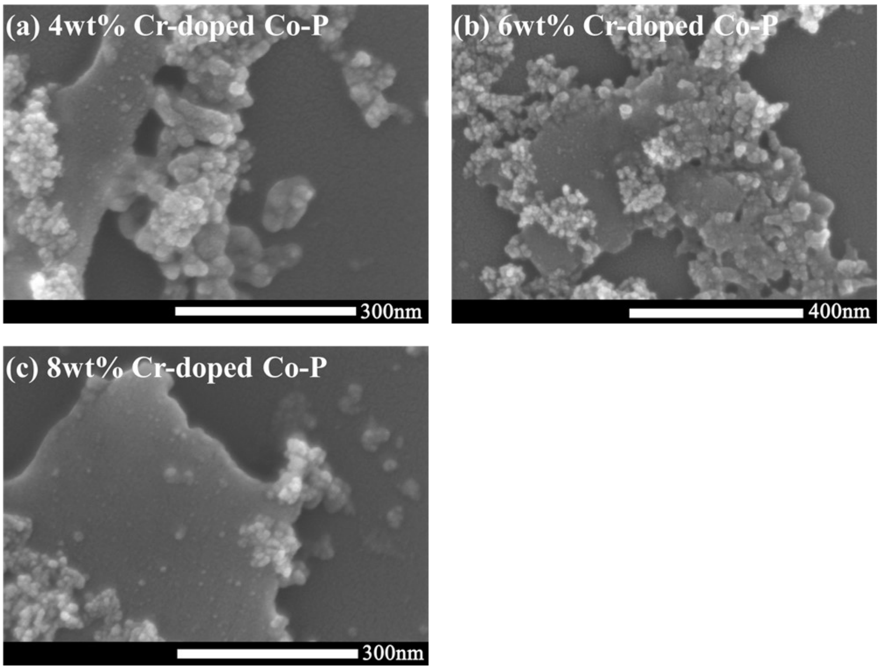

Fig. S17. SEM images of (a) 4, (b) 6 and (c) 8wt% Cr-doped Co-P.

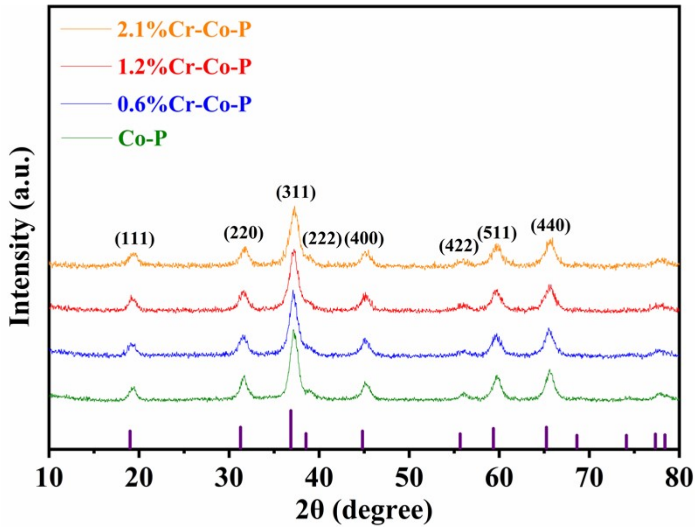

Fig. S18. XRD patterns of M% Cr-Co-P (PDF#42-1467).

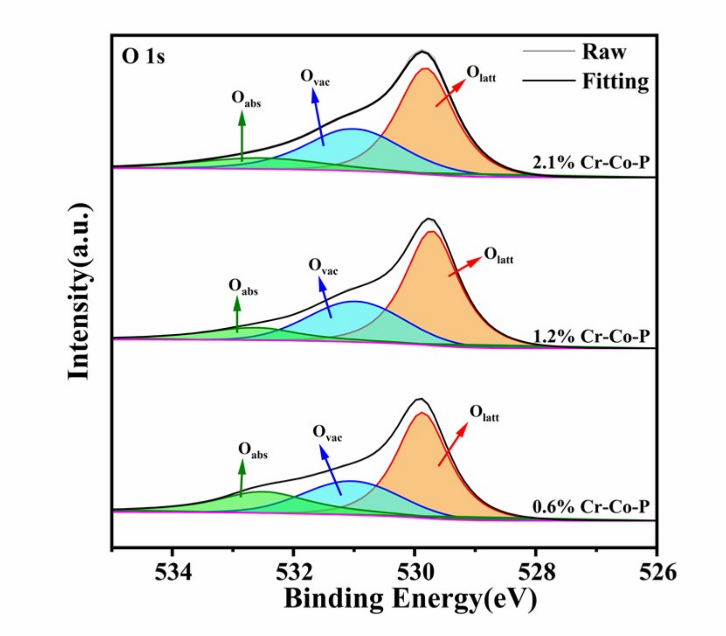

Fig. S19. O 1s XPS spectra of M% Cr-Co-P

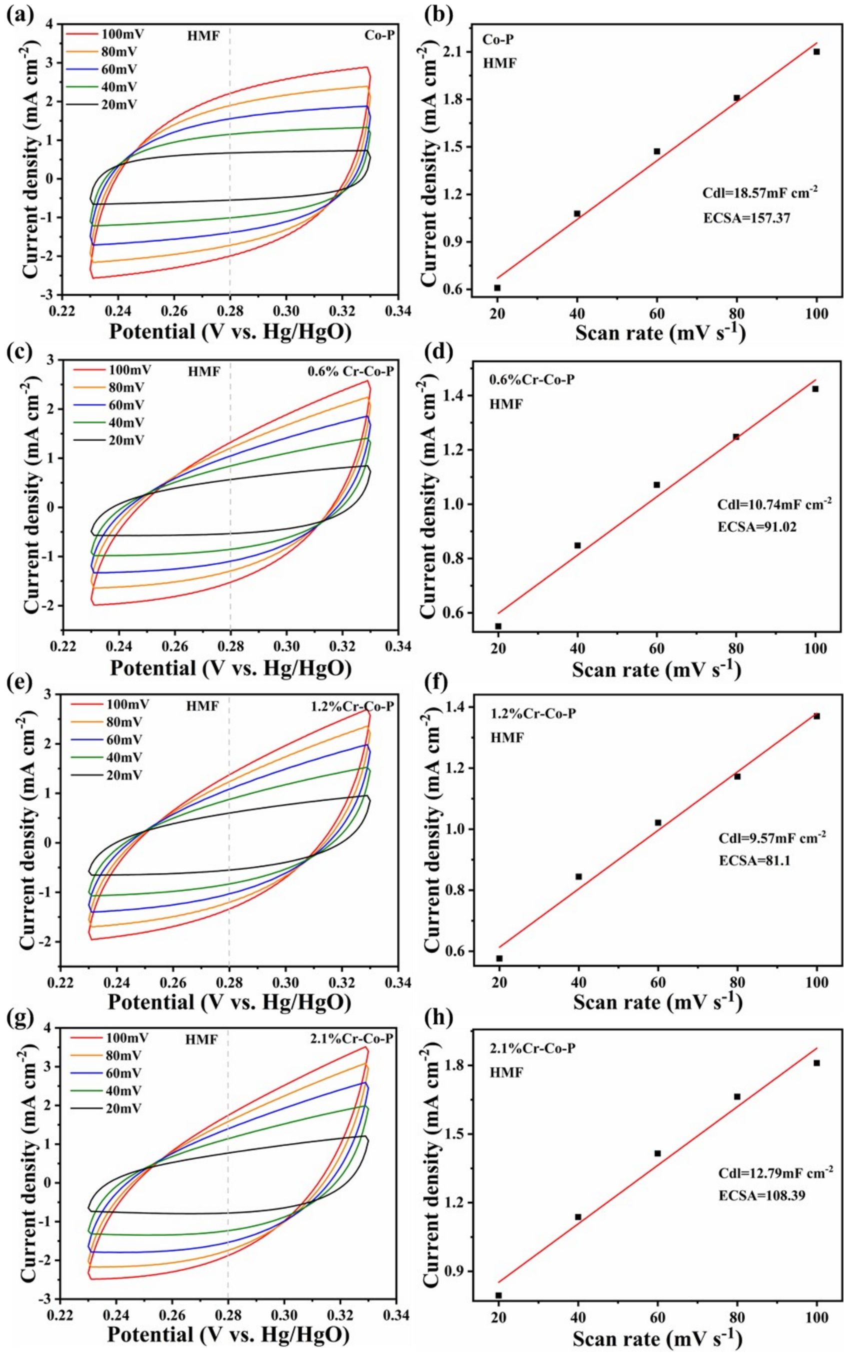

Fig. S20. Cyclic voltammograms (CVs) obtained with Co-P (a), 0.6% Cr-Co-P (c), 1.2% Cr-Co-P (e) and 2.1% Cr-Co-P (g) in 1.0 M KOH with 10 mM HMF at scan rates of 20, 40, 60, 80 and 100 mV, respectively. Change of current density plotted against scan rate for Co-P (b), 0.6% Cr-Co-P (d), 1.2% Cr-Co-P (f) and 2.1% Cr-Co-P (h) in 1.0 M KOH with 10 mM HMF. The linear slope (b, d, f and h) is equivalent to the double-layer capacitance Cdl. The corresponding ECSA value is calculated via the equation ECSA = Cdl/Cs, where the specific capacitance value (Cs) was 118 μF cm^{-2}.

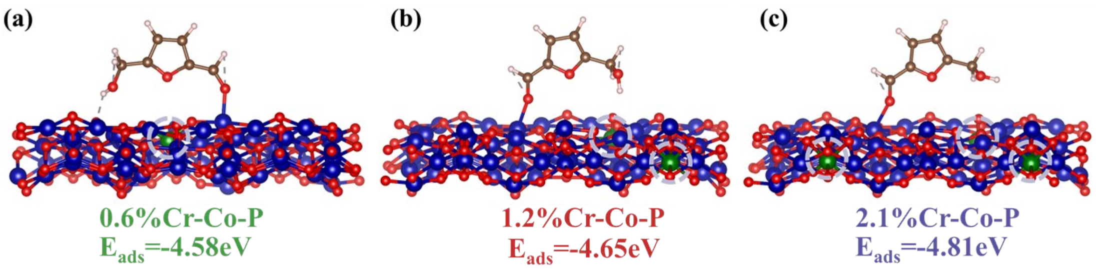

Fig. S21. Figures (a) to (c) show the optimal adsorption configuration and energy (E_{ads}) of HMF on 0.6% Cr-Co-P, 1.2% Cr-Co-P and 2.1% Cr-Co-P obtained by DFT calculations (Absorption site only on Co). The blue, green, red and white spheres represent Co, Cr, O and H, respectively. Using 1 Cr atom, 2 Cr atoms, and 3 Cr atoms to indicate the increase in doping concentration.

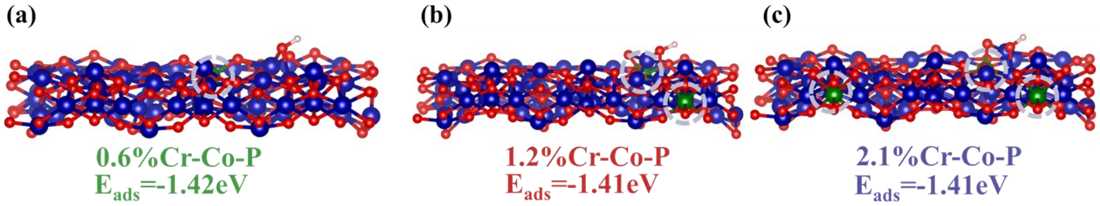

Fig. S22. Figures (a) to (c) show the optimal adsorption configuration and energy (E_{ads}) of OH^- on 0.6% Cr-Co-P, 1.2% Cr-Co-P and 2.1% Cr-Co-P obtained by DFT calculations (Absorption site only on Co). The blue, green, red and white spheres represent Co, Cr, O and H, respectively. Using 1 Cr atom, 2 Cr atoms, and 3 Cr atoms to indicate the increase in doping concentration.

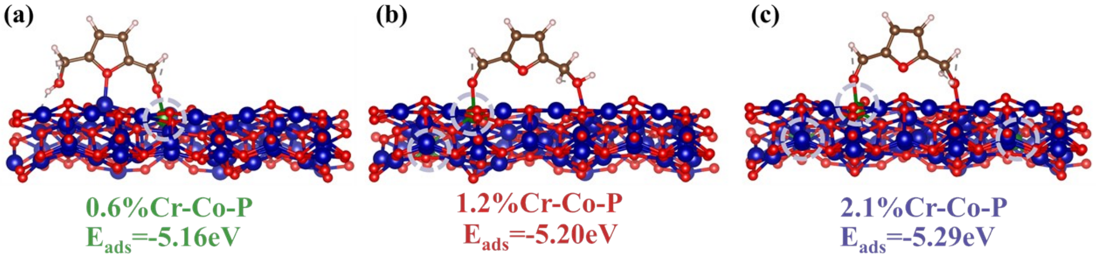

Fig. S23. Figures (a) to (c) show the optimal adsorption configuration and energy (E_{ads}) of HMF on 0.6% Cr-Co-P, 1.2% Cr-Co-P and 2.1% Cr-Co-P obtained by DFT calculations (Absorption site on Cr). The blue, green, red and white spheres represent Co, Cr, O and H, respectively. Using 1 Cr atom, 2 Cr atoms, and 3 Cr atoms to indicate the increase in doping concentration.

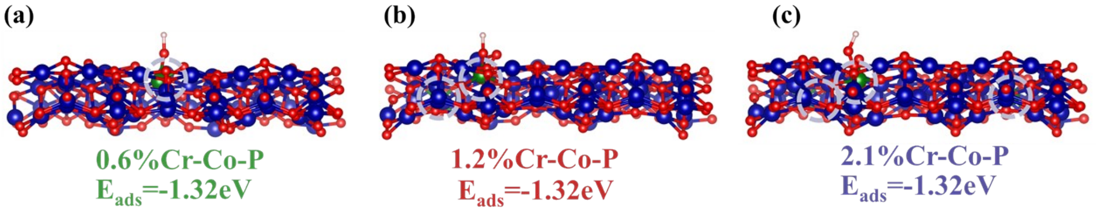

Fig. S24. Figures (a) to (c) show the optimal adsorption configuration and energy (E_{ads}) of OH^- on 0.6% Cr-Co-P, 1.2% Cr-Co-P and 2.1% Cr-Co-P obtained by DFT calculations (Absorption site on Cr). The blue, green, red and white spheres represent Co, Cr, O and H, respectively. Using 1 Cr atom, 2 Cr atoms, and 3 Cr atoms to indicate the increase in doping concentration.

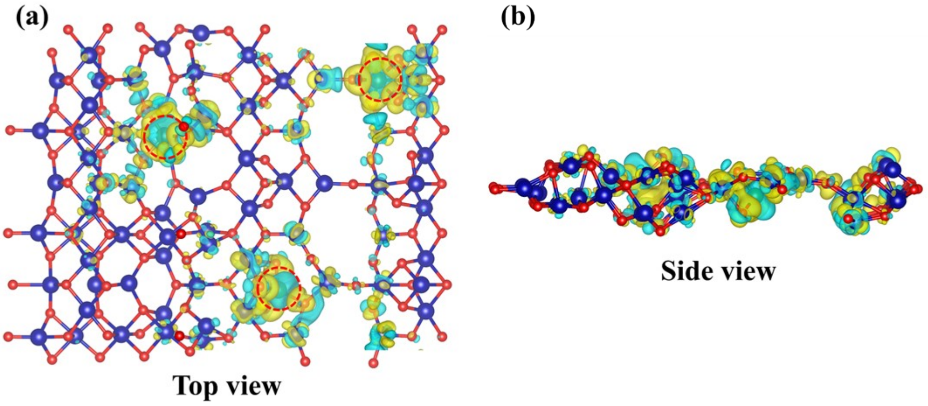

Top view

Side view

Fig. S25. Charge density difference on Cr-doped Co_3O_4 nanoparticle.

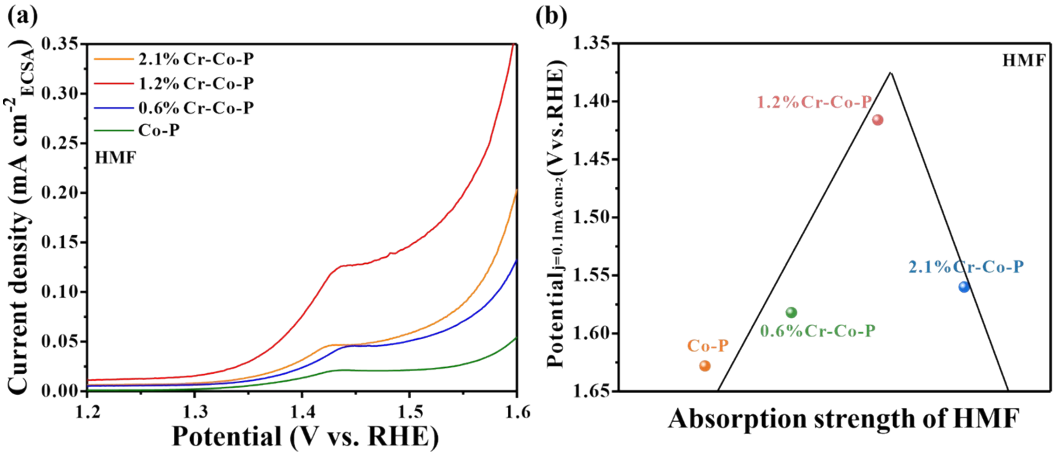

Fig. S26. (a) The LSV curves of M% Cr-Co-P by ECSA normalization at a scan rate of 5 mV s^{-1} in 1.0 M KOH with 10 mM HMF. (b) The volcanic plot of HMF electrooxidation on M% Cr-Co-P after ECSA normalization.

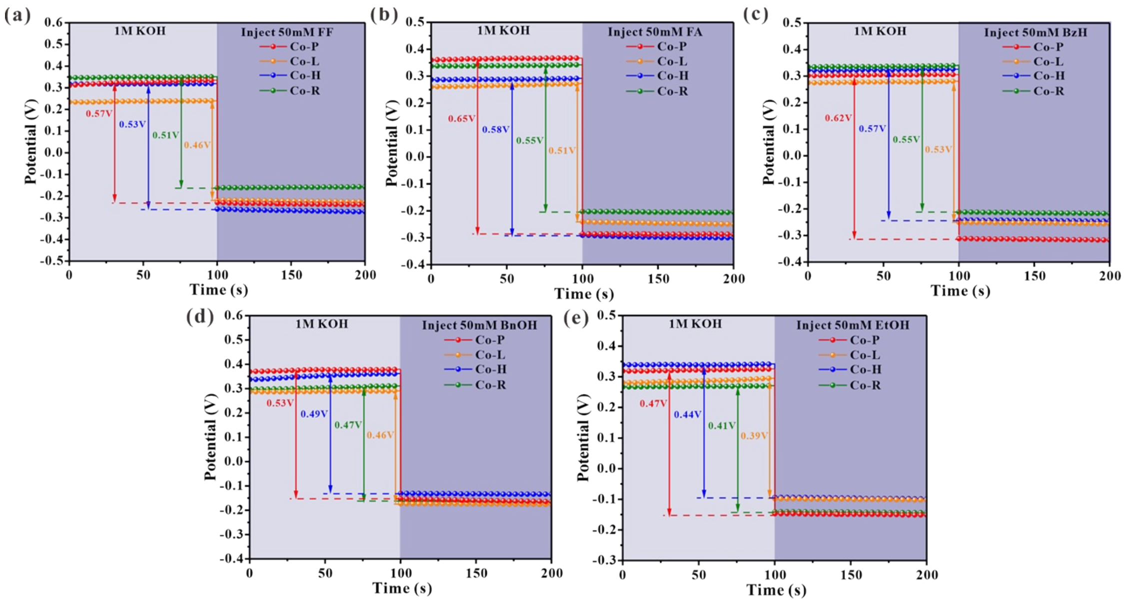

Fig. S27. The OCP curves of Co_3O_4 NCs in 1.0 M KOH and 50 mM FF (a), FA (b), BzH (c), BnOH (d) and EtOH (e) was injected subsequently.

2. Supplementary Tables

Table S1. XPS results of Co_3O_4 NCs.

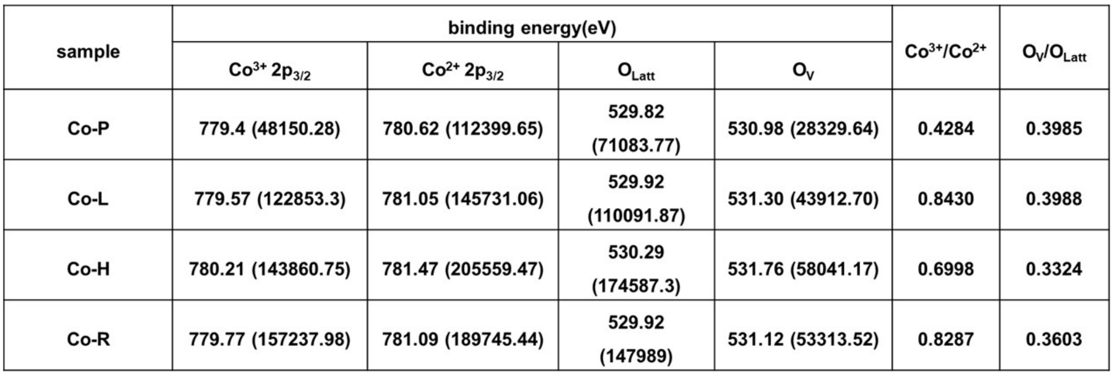

sample	binding energy(eV)				Co^{3+}/Co^{2+}	O_V/O_{Latt}
	Co^{3+} $2p_{3/2}$	Co^{2+} $2p_{3/2}$	O_{Latt}	O_V		
Co-P	**779.4 (48150.28)**	**780.62 (112399.65)**	**529.82 (71083.77)**	**530.98 (28329.64)**	**0.4284**	**0.3985**
Co-L	**779.57 (122853.3)**	**781.05 (145731.06)**	**529.92 (110091.87)**	**531.30 (43912.70)**	**0.8430**	**0.3988**
Co-H	**780.21 (143860.75)**	**781.47 (205559.47)**	**530.29 (174587.3)**	**531.76 (58041.17)**	**0.6998**	**0.3324**
Co-R	**779.77 (157237.98)**	**781.09 (189745.44)**	**529.92 (147989)**	**531.12 (53313.52)**	**0.8287**	**0.3603**

Table S2. ICP-OES analysis in 0.6% Cr-Co-P, 1.2% Cr-Co-P and 2.1% Cr-Co-P, respectively.

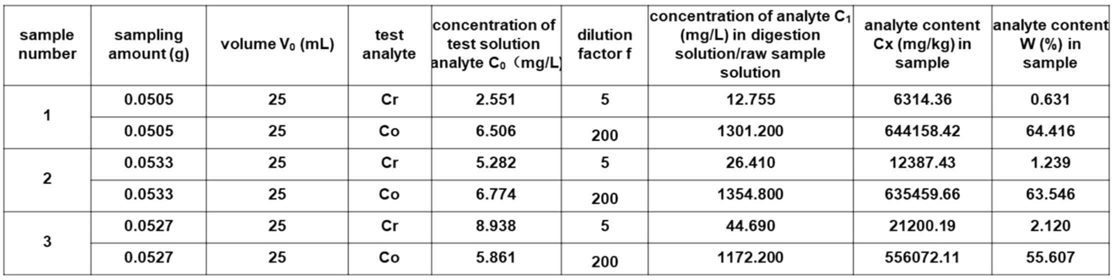

sample number	sampling amount (g)	volume V_0 (mL)	test analyte	concentration of test solution analyte C_0（mg/L)	dilution factor f	concentration of analyte C_1 (mg/L) in digestion solution/raw sample solution	analyte content Cx (mg/kg) in sample	analyte content W (%) in sample
1	0.0505	25	Cr	2.551	5	12.755	6314.36	0.631
	0.0505	25	Co	6.506	200	1301.200	644158.42	64.416
2	0.0533	25	Cr	5.282	5	26.410	12387.43	1.239
	0.0533	25	Co	6.774	200	1354.800	635459.66	63.546
3	0.0527	25	Cr	8.938	5	44.690	21200.19	2.120
	0.0527	25	Co	5.861	200	1172.200	556072.11	55.607

Table S3. O 1s XPS spectra results of prepared catalysts.

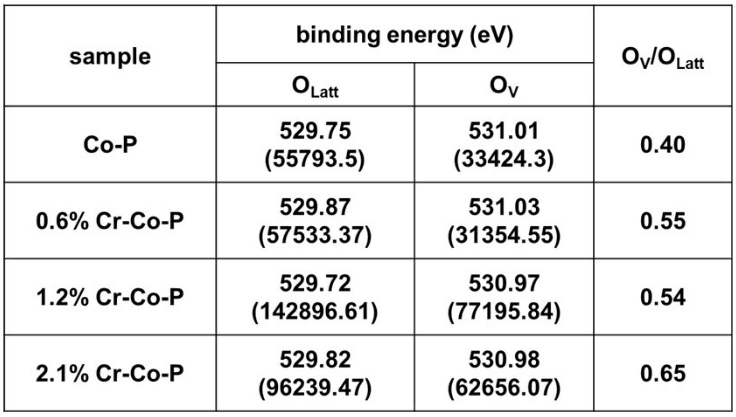

sample	binding energy (eV)		O_V/O_{Latt}
	O_{Latt}	O_V	
Co-P	529.75 (55793.5)	531.01 (33424.3)	0.40
0.6% Cr-Co-P	529.87 (57533.37)	531.03 (31354.55)	0.55
1.2% Cr-Co-P	529.72 (142896.61)	530.97 (77195.84)	0.54
2.1% Cr-Co-P	529.82 (96239.47)	530.98 (62656.07)	0.65